Transition From Surface Cavity Mode to Cavity Mode in Deep-Grooved Parallel Plate Waveguide

Yiming Zhu, Qingyun Sun, Jiaming Xu, and Lin Chen

***Abstract*—The parallel plate waveguide (PPWG) is an excellent device for guiding and controlling at terahertz wave. When a deep groove is integrated into a PPWG, only the surface cavity mode is excited, which limits its applications in filtering and sensing. In this paper, we demonstrated that in a double deep-grooved PPWG, both fundamental and higher-order cavity modes can be observed. Our experimental and simulation results show that the effective groove depth of the fundamental cavity mode in the bottom deep groove can be efficiently increased by cutting another shallow groove in the top metal plate, facing the bottom deep groove. In addition, the transition from the so-called surface cavity mode to traditional cavity mode can be observed with increasing depth of the shallow groove. These results may have applications in the multichannel filtering and sensing field.**

***Index Terms*—Terahertz wave, parallel plate waveguide, cavity mode, deep groove.**

I. Introduction

With increasing research in the terahertz (THz) field, many applications of THz have been found from basic science to security inspection, medical imaging, and astronomy in recent years [1]–[6]. The low-loss, undistorted THz pulse propagation in a parallel-plate waveguide (PPWG) has been widely used in the field of THz in the past decade [7]. Based on the excellent platform of the PPWG, several designs for transverse magnetic (TM) [8]–[10] and transverse electric (TE) [11]–[15] polarizations with resonant structure have recently been published. In particular, a THz microfluidic sensor based on PPWG with one groove has been presented [12]. By exciting the cavity mode in a groove embedded within a PPWG, a narrow resonance dip can be observed [13], [14] in the transmission spectrum [12]. We note that all of the above work focused on a shallow groove (the depth of the groove is the same as (similar to) the width of the groove). The deep-grooved PPWG has not been sufficiently studied because radiation cannot efficiently penetrate into the deep groove, resulting in a similar resonance mode to the shallow groove. Here, we call this type of cavity mode the "surface cavity mode" [15]. In this paper, we report on a new method to increase the field in a deep groove by adding another shallow groove in the top plate, directly facing the original bottom deep groove. By measuring the transmission properties of PPWGs with double cavities of different depths, we found that the field of the fundamental cavity mode can penetrate into the deep groove if the top cavity has suitable depth, while it can hardly occur in a structure with only a single deep cavity. In addition, we also observed the transition from the surface cavity mode to the conventional cavity mode. Meanwhile, more cavity modes will emerge and the resonant frequency of fundamental cavity mode will remain unchanged with increasing top groove depth. The fundamental and higher-order cavity modes may have potential applications in multichannel filtering and sensing.

Manuscript received May 23, 2016; revised July 15, 2016; accepted August 3, 2016. This work was supported in part by the National Program on Key Basic Research Project of China (973 Program) under Grant 2014CB339806, in part by the Basic Research Key Project under Grant 12JC1407100, in part by the Major National Development Project of Scientific Instrument and Equipment under Grants 2011YQ150021 and 2012YQ14000504, in part by the National Natural Science Fundation of China under Grants 61138001, 61205094, 61671302 and 61307126, in part by the Shanghai Rising-Star Program under Grant 14QA1403100, in part by the Program of Shanghai Subject Chief Scientist under Grant 14XD1403000, in part by the Scientific Research Innovation Project of the Shanghai Municipal Education Commission under Grant 14YZ093, and in part by the New Century Excellent Talents Project from the Ministry of Education under Grant NCET-12-1052.

Y. Zhu is with the Shanghai Key Laboratory of Modern Optical Systems, Engineering Research Center of Optical Instrument and Systems, Ministry of Education, University of Shanghai for Science and Technology, Shanghai 200093, China, and also with the Cooperative Innovation Centre of Terahertz Science, University of Electronic Science and Technology, Chengdu 611731, China (e-mail: ymzhu@usst.edu.cn).

Q. Sun and J. Xu are with the Shanghai Key Laboratory of Modern Optical Systems, Engineering Research Center of Optical Instrument and Systems, Ministry of Education, University of Shanghai for Science and Technology, Shanghai 200093, China (e-mail: 583199081@qq.com; 42123652@qq.com).

L. Chen is with the Shanghai Key Laboratory of Modern Optical Systems, Engineering Research Center of Optical Instrument and Systems, Ministry of Education, University of Shanghai for Science and Technology, Shanghai 200093, China, with the Cooperative Innovation Centre of Terahertz Science, University of Electronic Science and Technology, Chengdu 611731, China, and also with the Ultrafast THz Optoelectronic Laboratory, Oklahoma State University, Stillwater, USA (e-mail: linchen@usst.edu.cn).

Color versions of one or more of the figures in this paper are available online at http://ieeexplore.ieee.org.

Digital Object Identifier 10.1109/JSTQE.2016.2598605

II. Experiment and Results

The PPWG in this paper is similar to the metal/dielectric/metal (MDM) structure [16] in the visible range, and we use copper and air as the metal and dielectric material. As shown in Fig. 1(a), there are two cavities located symmetrically on both sides of the top and bottom plates. The bottom cavity has a depth h_2 of 1400 μm and width w of 400 μm. The top cavity has the same width, but the depth h_1 takes various values: 0 μm., 200 μm., 400 μm., 600 μm. and 800 μm. The gap spacing between the two plates d is *fixed* at 800 μm. In the real sample, a double-cylinder waveguide coupler is used to enhance the relative amplitude of the transmission [15], and there are two identical grooves on the coupler, which is perpendicular to the propagation direction of the THz wave, making it easy to change the depths of the cavities by substituting different metal blocks.

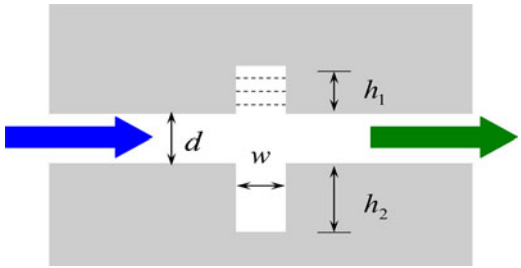

Fig. 1. Schematic drawing with main dimensions of the sample.

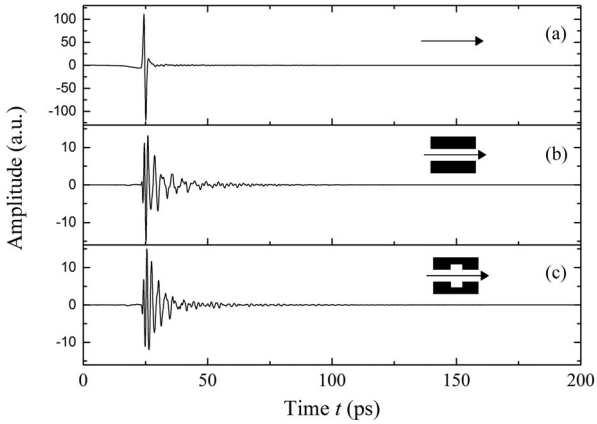

Fig. 2. The waveforms of different THz signals:(a) measurement in dry air without sample, (b) sample without cavity (reference), (c) sample with cavities (represented by $h_1 = 800\,\mu$m.)

The length, width and height of the two grooves are 50 mm, 5 mm and 3 mm, respectively. There are also two micrometers to finely adjust the displacement of the cavities and the gap spacing.

In the experiment, the resonant behavior of this PPWG structure is observed using a commercial THz time domain spectroscopy system (THz-TDS). The details of the experiment settings are the same as described in our previous work [15]. The waveforms obtained in the time domain are shown in Fig. 2. We used the signal of the sample with no cavity (Fig. 2(b)) as the reference and used the common divisor to calculate the transmissivities rather than the signal with no sample (Fig. 2(a)). The sampling time of the THz-TDS is approximately 200 *ps* in the time domain; that is, after the fast Fourier transform (FFT), the frequency resolution is approximately 5 GHz. Additional oscillating attenuation tails are also observed in Fig. 2(b) and (c) by inserting the structures, which may come from band stop below cutoff frequencies and resonances induced by cavities.

After data processing, the resonant behaviors of our sample are as shown in Fig. 3. The left column of Fig. 3 shows the input and output spectra obtained for different top cavity depths h_1. It can be clearly seen that there exist low-frequency cutoffs of the TE_1 modes at a frequency of shown 0.1875 THz, which is determined by the gap spacing $d = 800\,\mu$m. The blue lines represent the FFT of the reference signal (Fig. 2 (b)), so they are identical for the left panels in Fig. 3. The right column of Fig. 3 shows the corresponding transmission curves determined in experiments (dotted lines) for different top cavity depths h_1, compared with their counterparts obtained in simulation (solid lines). The measured data were extended to 1.5 ns by adding zeros at the end of the data, allowing the numbers of transmission dips to be clearly distinguished according to the curves. With increasing bottom cavity depth h_2, more cavity modes can be observed.

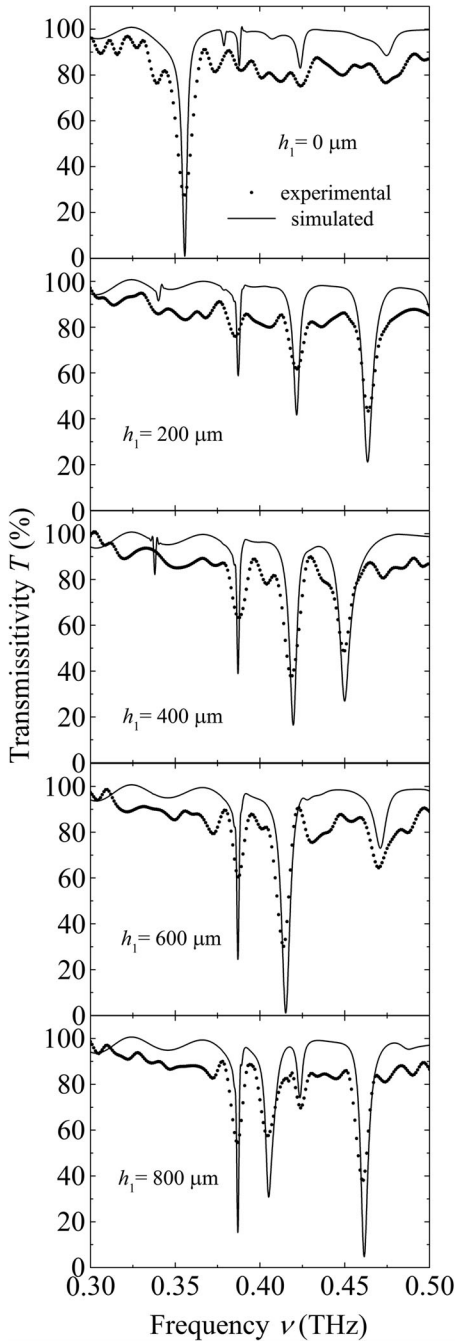

Fig. 3. Resonant transmission behaviors of our sample. *Left column*: measured input and output spectra: *blue*: input spectra (reference, all identical) *green*: output spectra (sample). *Right column*: transmission curves for different groove depths h_1, (a) $h_1 = 0\,\mu$m, (b) $h_1 = 200\,\mu$m, (c) $h_1 = 400\,\mu$m, (d) $h_1 = 600\,\mu$m, (e) $h_1 = 800\,\mu$m; *dotted lines*: experimental data, *solid lines*: simulated results.

III. Analysis and Discussion

A. Formation and Transition of Modes

To understand the effect of the continuously varied top cavity depth h_1, numerical simulations were performed using a

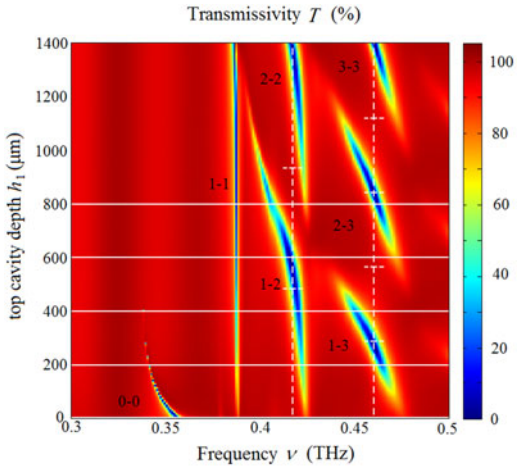

Fig. 4. 2D map of the transmissivity T versus the frequency ν and the top cavity depth h_1. *Horizontal white solid lines*: the depths h_1 investigated in our experiment. *Vertical white dashed lines*: the central frequencies of the "*m*-2" and "*m*-3" series of cavity modes. *Horizontal white short dashed lines*: trisection and quinquesection of $h_2 = 1400$ μm. *Black marks*: indicate the order of different cavity modes.

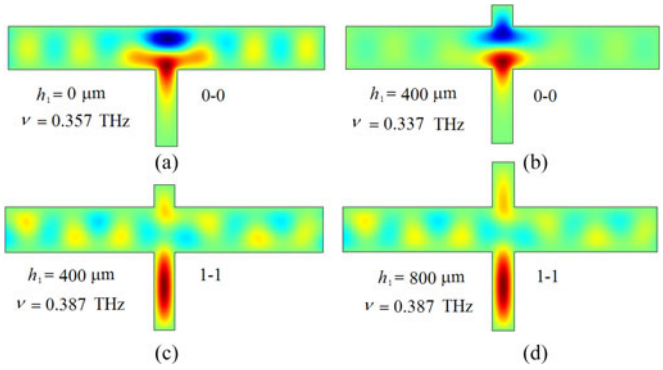

Fig. 5. Electrical field distributions in cavities of "0-0" and "1-1" modes. (a) & (b), "0-0" mode, (c) & (d) "1-1" mode.

commercial software package based on the finite element method (FEM) [15]. In the simulation, the parallel plates with resonant cavities are defined by the Drude model [17]–[20], and we used a perfectly matched layer (PML) to eliminate the boundary reflection. Under the condition that the bottom cavity depth h_2 and the air gap spacing d are fixed at 1400 μm and 800 μm, respectively, we obtained the transmissivity of the PPWG T versus the frequency ν and the bottom cavity depth h_2, as shown in Fig. 4 as a two-dimensional (2D) map.

Obviously, there exist seven modes and four series from the low frequency to the high frequency, which can be distinguished in the 2D map. To facilitate the discussion of these modes, we denote them using the symbols "*m*-*n*". The numbers m and n in these notations stand for the number of standing wave antinodes (maximum displacement in standing wave) in the top and bottom cavities, respectively, which can be inferred from the electrical field distributions of these modes (Figs. 5 and 6). In particular, we use "0-0" to represent the mode of the lowest frequency, for which no standing wave is formed in either the top

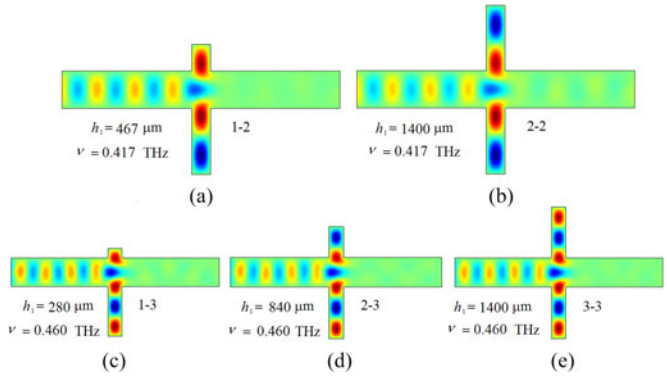

Fig. 6. Electrical field distributions in cavities of "*m*-2" and "*m*-3" series of cavity modes. (a) "1-2" (b) "2-2" (c) "1-3" (d) "2-3" (e) "3-3".

or the bottom cavity. The five horizontal white solid lines in the map represent the depths h_1 investigated in the experiment. As shown in Fig. 3 (right column), our experimental and simulation results agree well with each other except for the "0-0" mode. Its mode bandwidth is narrower than the frequency resolution of our THz-TDS, and therefore this mode cannot be identified experimentally.

According to Fig. 3, when the top cavity depth h_1 is equal to 0 μm, where the PPWG consists of a single deep cavity structure, there is only one mode ("0-0" mode) in the frequency range from 0.3 THz to 0.5 THz. Fig. 5(a) shows the electrical field distributions of the "0-0" mode for $h_1 = 0$ μm. We noted that the "0-0" mode is an invert-phase coupling mode, and the majority of its energy does not enter the space of the bottom cavity but only gathers at the interface between the transmission channel (spacing gap) and the cavity. Therefore, the mode should be classified as a surface cavity mode compared to the traditional cavity mode. Due to the great depth of the bottom cavity, it is difficult for the electromagnetic wave of this mode to change its propagation direction to enter the cavity, and hence the effective depth is very short (approximately 1/3 of the bottom cavity). As the top cavity depth h_1 increases, the electromagnetic wave can partially enter the top cavity but still remains largely restricted in the interfaces of two cavities (shown in Fig. 5(b)). As the top cavity depth increases further, a red shift of the central frequency of the "0-0" mode is observed (shown in Fig. 4) because of the increase in the optical path. However, the extent of the red shift remains unchanged for a range of depths (200 μm to 400 μm.) due to the anti-symmetry property of this mode. As the top cavity depth continues to increase, the growing symmetry feature of the two cavities dampens the formation of the invert-phase mode. As a result, the "0-0" mode gradually becomes weaker and finally disappears (above 400 μm). Due to the destruction interference condition (because our device is a notch filter), the phase change of the surface cavity mode's electronic field between two cavity interfaces should be an odd integer-multiple of π, i.e., $(2k+1)\pi$. In Fig. 5(a) and (b), for the "0-0" mode, the electronic field phase changes only by π (from blue to red) for the condition of $k = 0$. Furthermore, according to the theory of mode coupling, the energy of the asymmetrical coupling is intrinsically lower than the energy of symmetrical cou-

pling, and therefore the surface cavity mode occurs at the lowest frequency.

In contrast, when the top cavity depth h_1 is not equal to 0 μm., three series of modes appear that do not exist in the single-cavity structure ($h_1 = 0\,\mu$m). According to Fig. 5(c), (d) and Fig. 6, all these novel modes are traditional cavity modes, whose energy can enter and fill the entire space of the bottom cavity. In these cases, the effective depth is equal to the full depth of the bottom cavity. This extraordinary phenomenon can be explained by the electromagnetically induced transparency (EIT) effect [17], [18]. According to waveguide theory, if only one deep cavity exists in the PPWG, the bottom cavity is too deep for electromagnetic waves to propagate in it, so only the surface cavity mode can be observed in the single-cavity structure (Figs. 4 and 5(a)). However, if there is another cavity in a symmetric position with respect to the deep cavity, the electromagnetic wave can change direction, enter shallowly to form a standing wave in the vertical direction and eventually fill both cavities. Even if the two cavities have the same large depth ($h_1 = h_2 = 1400\,\mu$m.), the standing wave can form because the top cavity significantly changes the boundary condition (top of Fig. 4). Due to the interference conditions, the phase change of the electronic field from the top cavity boundary to the bottom cavity boundary should be an integer-multiple of π, i.e., $k\pi$. In other words, the space extension of the standing wave must be an integer-multiple of wave node $k\lambda/2$. Considering that the propagating wave already occupies one half-wavelength in transmission vertically and that one cavity must contain at least one node to form the standing wave, the integer k must be greater than or equal to 3 for the cavity mode to occur. In terms of the notation "*m*-*n*", the integer k should be equal to $m + n + 1$. As the top cavity depth h_1 increases, the optical path is elongated remarkably. As a result, the cavity modes show a red shift to achieve longer wave nodes or become higher order to allow more wave nodes to fill the cavities (Fig. 4)

B. Periods of Higher Cavity Modes

In Fig. 4, the locations of the high-order cavity modes show clear periods between them. These high-order modes can be grouped into 2 mode series, "*m*-2" and "*m*-3", with the two frequency ranges of 0.395–0.425 THz and 0.440–0.475THz, respectively. The vertical white dashed lines of Fig. 4 represent the central frequencies of the "2-2" and "3-3" modes when the structure is perfectly symmetrical ($h_1 = h_2 = 1400\,\mu$m). We also calculated the top cavity depths h_1 of the "1-2", "1-3" and "2-3" modes, which have the same central frequencies as the ones indicated by the vertical white dashed lines. The corresponding electrical field distributions are shown in Fig. 6. Under the condition that the bottom cavity depth h_2 is fixed at 1400 μm, when stable cavity mode is excited, the resonant wavelength (frequency) is determined by the wave nodes n in the bottom cavity. Then, the top cavity depth h_1 only determines the wave nodes m in the top cavity and has nothing to do with resonant wavelength (frequency). The field distributions of modes of the same series are very similar except that there is an additional standing wave node in the top cavity. The top cavity depth h_1 of the "*m*-*n*" modes at the frequencies mentioned is determined to be

$$h_1 = \frac{2m-1}{2n-1} h_2. \tag{1}$$

For the "m-2" and "m-3" mode series, the denominators are 3 and 5, so we indicate the trisection and quinquesection of h_2 by horizontal white short dashed lines in Fig. 4. It is clear that the odd trisection and quinquesection (1/3, 3/3, 1/5, 3/5 and 5/5) are the positions where the cavity modes are strongest, while the even trisection and quinquesection (0/3, 2/3, 0/5, 2/5 and 4/5) are the positions where the cavity modes are weakest and can be considered as the boundaries between these cavity modes. At other frequencies, additional similar periodicities can also be found. This feature can find potential applications in tunable channel switches due to the rigorous periodical frequency change.

IV. Conclusion

This work demonstrates the transmission properties of a PPWG with double cavities of various top cavity depths by both experimental and simulation methods. We distinguished two different types of modes in our sample, cavity modes and interface modes and discussed the mechanisms and features of their formation. The results indicate that the cavity modes are generated by the standing waves between the cavity boundaries and show a red shift with increasing cavity depth. Meanwhile, the surface cavity mode corresponds to the asymmetrical coupling in the interface and does not depend on the cavity depth. Further study revealed that the traditional cavity modes appear for the double-cavity structure, and the interface mode is actually a regression of the single-cavity mode. Some interesting features of the unchanged cavity mode and the periodically altering cavity modes provide new ideas for the development of sensors and switches in the terahertz band.

Acknowledgment

The authors would like to thank Prof. Yi Liu from École Poly Technique, Université Paris-Saclay, France for his contributions to the manuscript.

References

[1] M. Tonouchi, "Cutting-edge terahertz technology," *Nature Photon.*, vol. 1, pp. 97–105, 2007.

[2] M. Gerhard, C. Imhof, and R. Zengerle, "Low-loss compact high-Q 3D THz grating resonator based on a hybrid silicon metallic slit waveguide," *Opt. Express*, vol. 18, 2010, Art. no. 11707.

[3] L. Chen *et al.*, "Mode splitting transmission effect of surface wave excitation through a metal hole array," *Light Sci. Appl.*, vol. 2, 2013, Art. no. e60.

[4] P. A. George, C. Manolatou, F. Rana, A. L. Bingham, and D. R. Grischkowsky, "Integrated waveguide-coupled terahertz microcavity resonators," *Appl. Phys. Lett.*, vol. 91, 2007, Art. no. 191122.

[5] A. L. Bingham and D. Grischkowsky, "Terahertz two-dimensional high-Q photonic crystal waveguide cavities," *Opt. Lett.*, vol. 33, pp. 348–350, 2008.

[6] L. Chen, Y. M. Wei, X. F. Zang, Y. M. Zhu, and S. L. Zhuang, "Excitation of dark multipolar plasmonic resonances at terahertz frequencies," *Sci. Rep.*, vol. 6, 2016, Art. no. 22027.

[7] R. Mendis and D. Grischkowsky, "Undistorted guided-wave propagation of subpicosecond terahertz pulses," *Opt. Lett.*, vol. 26, pp. 846–848, 2001.

[8] E. S. Lee and T. I. Jeon, "Tunable THz notch filter with a single groove inside parallel-plate waveguides," *Opt. Express*, vol. 20, pp. 29605–29612, 2012.
[9] E. S. Lee *et al.*, "Terahertz band gaps induced by metal grooves inside parallel-plate waveguides," *Opt. Express*, vol. 20, pp. 6116–6123, 2012.
[10] S. Harsha, N. Laman, and D. Grischkowsky, "High-Q terahertz Bragg resonances within a metal parallel plate waveguide," *Appl. Phys. Lett.*, vol. 94, 2009, Art. no. 091118.
[11] R. Mendis and D. M. Mittleman, "An investigation of the lowest-order transverse-electric (TE1) mode of the parallel-plate waveguide for THz pulse propagation," *J. Opt. Soc. Amer. B*, vol. 26, pp. A6–A13, 2009.
[12] R. Mendis, V. Astley, J. Liu, and D. M. Mittleman, "Terahertz microfluidic sensor based on a parallel-plate waveguide resonant cavity," *Appl. Phys. Lett.*, vol. 95, 2009, Art. no. 171113.
[13] R. Mendis and D. M. Mittleman, "Comparison of the lowest-order transverse- electric (TE1) and transverse-magnetic (TEM) modes of the parallel-plate waveguide for terahertz pulse applications," *Opt. Express*, vol. 17, pp. 14839–14850, 2009.
[14] V. Astley, B. McCracken, R. Mendis, and D. M. Mittleman, "Analysis of rectangular resonant cavities in terahertz parallel-plate waveguides," *Opt. Lett.*, vol. 36, pp. 1452–1454, 2011.
[15] L. Chen *et al.*, "Controllable multiband terahertz notch filter based on a parallel plate waveguide with a single deep groove," *Opt. Lett.*, vol. 39, pp. 4541–4544, 2014.
[16] L. Chen *et al.*, "Observation of large positive and negative lateral shifts of a reflected beam from symmetrical metal-cladding waveguides," *Opt. Lett.*, vol. 32, pp. 1432–1434, 2007.
[17] L. Chen *et al.*, "Observation of electromagnetically induced transparency-like transmission in terahertz asymmetric waveguide-cavities systems," *Opt. Lett.*, vol. 38, pp. 1379–1381, 2013.
[18] L. Chen *et al.*, "Manipulating terahertz electromagnetic induced transparency through parallel plate waveguide cavities," *Appl. Phys. Lett.*, vol. 103, 2013, Art. no. 251105.
[19] Y. M. Zhu, C. M. Gao, and L. Chen, "Terahertz transmission properties of parallel-plate waveguide with double symmetrical resonant cavities," *Optical Instruments*, vol. 36, pp. 323–327, 2014.
[20] L. Chen, C. M. Gao, J. M. Xu, L. Xie, and Y. M. Zhu, "Terahertz transmission properties of sub-wavelength hole array and bull's eye structures on aluminum slab," *Optical Instruments*, vol. 35, pp. 1–6, 2013.

Yiming Zhu received the B.S. and M.S. degrees in applied physics from Shanghai Jiaotong University, Shanghai, China, in 2002 and 2004, respectively, and the Ph.D. degree in electronics engineering from the University of Tokyo, Tokyo, Japan, in 2008.

He is currently a Professor with the University of Shanghai for Science and Technology, Shanghai, China, and the Vice Director of the Shanghai Key Lab of Modern Optical System. He has published more than 70 papers on SCI journals.

Prof. Zhu received the Japanese Government (Monbukagakusho) Scholarship in 2004.

QingYun Sun was born in Jiangsu, China, in 1993. She received the B.S. degree from Nankai University, Tianjin, China, in 2014. She is currently working toward the M.S. degree at the University of Shanghai for Science and Technology, Shanghai, China. Her research interests include terahertz waveguides, broadband filters, and sensor chips.

Jiaming Xu was born in Shanghai, China, in 1989. He received the M.S. degree from the University of Shanghai for Science and Technology, Shanghai, China, in 2015. He is currently working toward the Ph.D. degree at the University of Texas at Austin, Austin, TX, USA. His research interests include terahertz waveguides and broadband filters.

Lin Chen was born in Jiangsu, China, in 1980. He received the B.S. and M.S. degrees in electrical engineering from Southeast University, Jiangsu, China, in 2002 and 2005, respectively, and the Ph.D. degree in optics from Shanghai Jiao Tong University, Shanghai, China, in 2008.

Since 2008, he has been with the College of Optical-Electrical and Computer Engineering, University of Shanghai for Science and Technology, Shanghai, China, where he is currently the faculty of communication engineering. From 2007 to 2008, he was with Avanex Corporation as Senior Engineer. From 2012 to 2013, he was a Visiting Scholar with the State Key Laboratory of Millimeter Waves (meta-group of Tie Jun Cui), Southeast University. He has currently been a Visiting Researcher with Ultrafast THz Optoelectronic Laboratory, Oklahoma State University, Stillwater, OK, USA. His research interests include terahertz waveguides, metamaterials, and labs on chips. He had been designated a "Chen Guang" Scholar in 2009, received the China Instrument Society Jin Guofan Youth Award in 2011, and designated a Shanghai "Rising Star" Scholar in 2014. He has published more than 50 SCI papers and 20 patents. As the Project Leader, he is also responsible for several national funding grants and grants supported by the Chinese and Shanghai government.